Time-dependent density-functional theory simulation of electron wave-packet scattering with nanoflakes

Keisuke Tsubonoya, Chunping Hu, and Kazuyuki Watanabe[*]

Department of Physics, Tokyo University of Science, 1-3 Kagurazaka, Shinjuku-ku, Tokyo 162-8601, Japan

Low-energy electron scattering with nanoflakes is investigated using a time-dependent density functional theory (TDDFT) simulation in real time and real space. By representing the incident electron as a finite-sized wave packet, we obtain diffraction patterns that show not only the regular features of conventional low-energy electron diffraction (LEED) for periodic structures but also special features resulting from the local atomic inhomogeneity. We have also found a signature of π plasmon excitation upon electron impact on a graphene flake. The present study shows the remarkable potential of TDDFT for simulating the electron scattering process, which is important for clarifying the local and periodic atomic geometries as well as the electronic excitations in nanostructures.

PACS number(s): 73.20.Mf, 61.05.jd, 31.15.ee, 61.46.−w

Time-dependent density functional theory [1,2] (TDDFT) has become a standard tool for studying the electronic states of excitations and nonequilibrium processes for many electron systems. Great achievements have been made, especially in the derivation of linear response properties such as optical absorption spectra [3–9] and nonadiabatic couplings [10], as well as simulations of real-time nonlinear electron dynamics under strong electric fields [11] or lasers [12]. However, there still remains an issue for TDDFT regarding elastic electron scattering. In terms of the response function, the scattering amplitudes of electron scattering from targets that can bind an extra electron can be rigorously extracted from the linear response TDDFT formalism [13,14]. Nevertheless, extending the treatment to bound-free correlation for low-energy electron scattering from polyatomic molecules is still necessary.

In this study we present a new method for TDDFT simulations of electron scattering, which involves representing the incident electron as a wave packet (WP) and evolving it using the time-dependent Kohn-Sham (TDKS) equations. The simulation is carried out in real time and real space, and the calculation procedure is a mimic of the experimental process for low-energy electron diffraction (LEED) [15]. As a widely used technique, LEED is a reliable and powerful tool for the determination of periodic surface structures [16]. By fitting simulated images to the experimentally obtained ones, based on the multislice finite difference method as an example, which accounts for multiple scattering with a full potential calculation [17], the surface atomic geometries can be clarified. Conventional LEED techniques, however, have to be used carefully for structures with aperiodic defects.

Recently a theoretical simulation method called NanoLEED, based on plane waves and developed for nano-material analysis [18,19], was shown to be suitable for the structural determination of isolated, finite-sized nanomaterials. Meanwhile, continuous efforts are being made to develop experimental techniques to reduce the electron-beam width, as demonstrated by a recent LEED experiment using the field emission from scanning tunneling microscopy tips [20].

Furthermore, a recent nanobeam electron diffraction (NBED) experiment by Hirata *et al.* shows that the electron beam can be converged to less than 1 nm in diameter and can be used to probe local structures of atomic clusters [21]. Therefore, representing the incident electrons as finite-sized WPs is a natural choice for the simulation of LEED patterns of nanostructures using a nanobeam.

In addition to the periodicity of nanostructures, the WP scattering approach can also capture information on the local atomic geometry, which is hard to detect through conventional LEED analysis with plane waves. Since electron WP scattering with nanostructures is essentially a time-dependent and local process, TDDFT simulations in real time and real space are an ideal computational tool for this purpose. The present TDDFT method considers a full dynamic description of both the target and incident electron, which is necessary for modeling nanostructures. Compared with the conventional scattering theory, the TDDFT method has an advantage in that multiple and inelastic scatterings are *automatically* included in the TDDFT framework. As the capability of real-time TDDFT simulations of electron-target scattering has not yet been demonstrated, assessing the applicability of TDDFT to this area is of great value. In addition to the simulation of diffraction patterns, the real-time TDDFT method is also expected to simultaneously elucidate the electronic excitations in the target upon electron impact.

In treating electron scattering with a target, the first step is to obtain information on the ground state of the target through static density functional theory (DFT) calculations [22,23]. Then a free electron described by a Gaussian WP is incident to the target, and the whole system is propagated in time by TDDFT. The ground-state density of the target is defined as $n^{\mathrm{TGT}}(\mathbf{r})$ and the incident WP is expressed as

$$\psi^{\mathrm{WP}}(\mathbf{r}) = \left(\frac{1}{\pi d^2}\right)^{\frac{3}{4}} \exp\left[-\frac{(\mathbf{r}-\mathbf{b})^2}{2d^2} + i\mathbf{k}\cdot\mathbf{r}\right], \quad (1)$$

where d, $\mathbf{b}$, $\mathbf{k}$ are respectively the standard deviation, center position and wave vector of the WP. We adopt atomic units in the following equations.

―――――
[*]kazuyuki@rs.kagu.tus.ac.jp

At time $t = 0$ the total electron density is given by

$$n(\mathbf{r},0) = n^{\text{TGT}}(\mathbf{r}) + |\psi^{\text{WP}}(\mathbf{r})|^2. \tag{2}$$

The wave functions $\psi_i(\mathbf{r},t)$ that belong to the target evolve in time according to the TDKS equation,

$$i\frac{\partial}{\partial t}\psi_i(\mathbf{r},t) = \left[-\frac{1}{2}\nabla^2 + \int \frac{n(\mathbf{r}',t)}{|\mathbf{r}-\mathbf{r}'|}d\mathbf{r}' + v_{\text{ion}}(\mathbf{r},\mathbf{t})\right.$$
$$\left. + v_{\text{xc}}(\mathbf{r},t)\right]\psi_i(\mathbf{r},t), \tag{3}$$

$$n(\mathbf{r},t) = \sum_{i=1}^{N/2} |\psi_i(\mathbf{r},t)|^2 + |\psi^{\text{WP}}(\mathbf{r},t)|^2, \tag{4}$$

where the index i runs from 1 to $N/2$ (N is the number of electrons in the target and the system is assumed to be spin unpolarized), v_{ion} is the ionic pseudopotential [24,25], and v_{xc} is the exchange-correlation potential. In our calculations we use the adiabatic local density approximation (ALDA) [26] here. The ALDA is known to have a drawback in terms of its description of electronic transport properties as shown in Refs. [27,28]. For optical absorption spectra of molecules and isolated clusters within the TDDFT scheme, however, the ALDA works well and the results are compatible with experiments, as discussed in Ref. [8]. It is also noted that in the literature the ALDA was applied to the study of secondary electron emission upon ion impact, and helium-ion microscopy images of graphene were successfully simulated [29]. Therefore, we expect the present results for the electron scattering of isolated nanostructures to be correct at least qualitatively, as discussed below.

The time evolution of the WP, $\psi^{\text{WP}}(\mathbf{r},t)$, is determined simultaneously by solving a TDKS equation similar to Eq. (3) except that $\psi_i(\mathbf{r},t)$ is replaced by $\psi^{\text{WP}}(\mathbf{r},t)$. The incident WP is not an exact eigenstate of a finite-sized box without the target but a free particle state with high kinetic energy (200 eV) in an infinite space at $t = 0$. A similar method has already been employed in simulations for ion-graphene scattering within TDDFT in Ref. [29] and in the time-dependent simulation of electron WP diffraction in a non-self-consistent crystal field [30]. The former work introduced an ion as a projectile in a vacuum and the latter gave reasonable transmission electron microscopy images and LEED intensities for bulk silicon and graphene using an electron WP.

Snapshots of the electron densities of the target-WP before and after the scattering are shown in Fig. 1. The calculation box is $18.4 \times 18.4 \times 31.7$ Å^3. A nanoflake target is placed in the center of the box and a propagating WP is shot from the right in the direction perpendicular to the flake plane [31,32]. We used the parameters $D = 6.35$ Å, $E_{\text{kin}} = \frac{1}{2}\mathbf{k}^2 = 100$–200 eV, and $d = 0.53$–3 Å for the incident WP. The distance 6.35 Å between the WP and the target is sufficient since there is no overlap of wave functions between them at $t = 0$. The observation plane for the diffraction pattern is also set at the incident position. We checked that the symmetry features of the LEED patterns did not change when larger distances were used. The only difference was that the images were enlarged and the intensity became faint. A similar distance of 8 Å between the target and the observation plane was used in the TDDFT simulation of helium-ion microscopy images in Ref. [29]. For the simulation
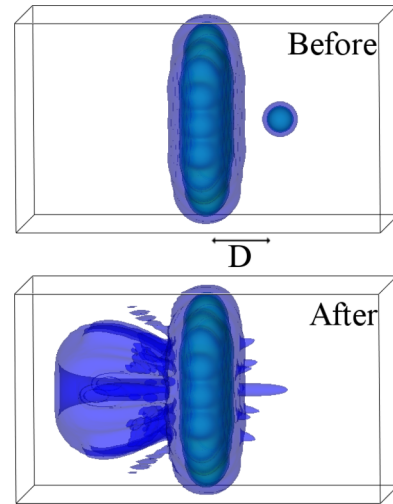
FIG. 1. (Color online) Snapshots of the electron densities of the target WP before and after the scattering. The WP is incident to the target from a distance D, at which an observation plane for the simulation of LEED patterns is also placed to capture the diffracted electrons.

of LEED patterns, a time step of $\Delta t = 4.84 \times 10^{-4}$ fs and a grid spacing of 0.16 Å are used, while in the calculation of the excitation spectrum, a larger time step of $\Delta t = 9.68 \times 10^{-4}$ fs is used. To propagate the KS wave functions, $\psi_i(\mathbf{r},t)$ and $\psi^{\text{WP}}(\mathbf{r},t)$, a fourth-order Taylor expansion is used [8,33]. The intensity of the electron diffraction pattern, $I(\mathbf{r})$, is obtained from the time integration of the total electron density, $n(\mathbf{r},t)$ of Eq. (4), on the observation plane (S) as

$$I(\mathbf{r}) = \int_{t_1}^{t_2} n(\mathbf{r},t)dt, \quad \mathbf{r} \in S, \tag{5}$$

where t_1 and t_2 are respectively the starting and ending times of the simulation. Simultaneously, the electronic excitations of the target upon the electron impact can be calculated from the Fourier transform of the dynamical dipole moment using $n^{\text{TGT}}(\mathbf{r},t)$, the first term of the right-hand side of Eq. (4), as follows [8]:

$$n^{\text{TGT}}(\mathbf{r},t) = \sum_{i=1}^{N/2} |\psi_i(\mathbf{r},t)|^2, \tag{6}$$

$$p_x(t) = \int d\mathbf{r}\, x n^{\text{TGT}}(\mathbf{r},t), \tag{7}$$

$$p_x(\omega) = \int_0^T dt\, p_x(t) e^{(i\omega+\Gamma/2)t}, \tag{8}$$

$$\sigma_x^d(\omega) = C\omega \Im p_x(\omega). \tag{9}$$

Here, p_x is the dipole moment and x denotes the direction perpendicular to the incident direction of the WP. T is the total simulation time of p_x, Γ is a damping factor, $C = 1/c\varepsilon_0$ (c is the speed of light and ε_0 is the permittivity of free space), and $\sigma_x^d(\omega)$ is the dipole excitation [34–37]. This is similar to the calculation procedure of optical absorption cross section when irradiated by an optical electric field in a δ-function

form [8]. It is known that there is a close connection between the interaction of fast moving charged particles with a material and photoabsorption: The effect of the fast charged particle traveling nearby a target can be regarded almost the same as that of white light illuminated on the target [38]. This connection has been used for the determination of optical oscillator strengths throughout the spectrum of generalized oscillator strength from electron collision cross-section data [39]. However, for the calculation of the optical absorption from the dipole response, the Fourier transform of the electric field is necessary for the clear definition of dynamic polarizability. For the present calculations, the electric field exerted by the incident electron is hard to estimate. On the other hand, we note that the Fourier transform of a δ-function-like electric field is just a constant; therefore, it should be interesting to compare the resonance peak positions of dipole response induced by electron impact with those in the optical absorption cross section.

For the simulation of the LEED patterns, the starting and ending times of the simulation are respectively estimated by the arrival of the WP at the nanoflake and the boundaries, which correspond to $t_1 = 0.077$ fs and $t_2 = 0.25$ fs, respectively. During the simulation the atomic positions are fixed since the time interval is very short and the ions do not have time to move. For the simulation of $\sigma_x^d(\omega)$, a very different procedure is used. When the WP hits the box boundaries, it is assumed that the WP will exit the box and have no further impact on the nanoflake; therefore, the successive time evolution of the nanoflake is carried out without the WP, i.e., $\psi^{WP}(\mathbf{r},t)$ in Eq. (4) is no longer taken into account in the TDDFT calculation. To eliminate the effect of the abrupt change in electronic density of the nanoflake upon electron impact, this simulation is continuously carried out for 10 000 steps, following which the tracking of p_x of the nanoflake starts and continues for 25 000 steps, and is then used for $\sigma_x^d(\omega)$.

In Fig. 2, the left panel shows three examples of target flakes: a coronene ($C_{24}H_{12}$) in (a), a double-layer (AA stacking) coronene in (b), and a circumcoronene in (c). The right panel shows the corresponding diffraction patterns from our TDDFT simulations. All the patterns consist of an outer sixfold array of spots, and an inner array of spots rotated 30° from the outer spots. This symmetry feature is consistent with that of the experimental LEED pattern of graphene [40,41]. From the center of the spots in the patterns and the Bragg diffraction condition, the C-C distances in (a), (b), and (c) are calculated and found to be the same value of 1.44 Å. In the left panel, these distances are set to be 1.42 Å. Concerning the difference in the bond lengths, it is noted that the calculated LEED spots are blurred, having finite width around the center, which is shifted from the ideal position due to the following two reasons: the WP having some k values around the mean value defined by the incident kinetic energy and part of the wavefront of the WP not being perfectly parallel to the target plane, both of which are different from the ideal situation of plane-wave scattering.

The intensities of the inner and outer LEED spots for single-layer graphene should be the same [40,41]; however, it is found that the intensity of the inner spots is lower than that of the outer spots in Fig. 2(a). There are two reasons for this difference. The first is the finite-sized flake with H termination. The scattering
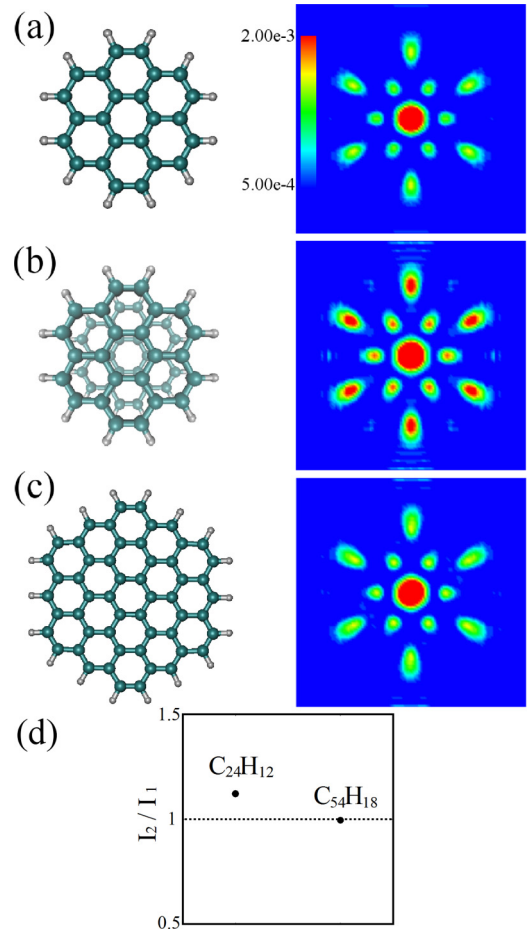
FIG. 2. (Color online) Target flakes (left) and the simulated diffraction patterns (right). (a) A coronene ($C_{24}H_{12}$), (b) a double-layer coronene, and (c) a circumcoronene ($C_{54}H_{18}$). The color scales are the same in the right panels. (d) The relative intensities of the outer spots (I_2) to the inner spots (I_1) for (a) and (b).

factor of H is smaller than that of carbon. The other is the finite-sized WP. The width of the WP on impact is comparable to the C-C bond length; thus, the WP electron only sees atoms in a limited area, not across the entire flake, and generates a diffraction pattern dependent on the local atomic geometry. Comparing (a) with (b), the spot intensity for the double layers in (b) is found to be larger than that for the single layer in (a). This feature is consistent with experimental observations of conventional LEED patterns of single- and double-layer graphene [40,41]. For AA-stacking double-layer graphene, the intensity of the outer spots is known to be twice as large as that of the inner spots. In (b), the intensity of the outer spots is larger than that of the inner spots; however, the ratio is not exactly 2. This is because the present flakes are finite-sized graphene with hydrogen termination. This finite-size effect can be further understood as the size of the graphene flake becomes larger from (a) to (c): The ratio of intensities between outer (I_2) and inner (I_1) spots decreases, and becomes closer to 1, which is the ideal value for the infinite graphene sheet, as shown in (d).

The above results show that if the symmetry of a honeycomb lattice can be represented by the local geometry of a finite
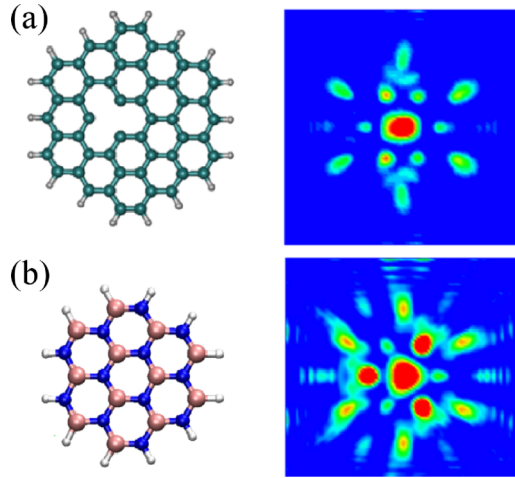
FIG. 3. (Color online) Target flakes (left) and the simulated diffraction patterns (right). (a) A circumcoronene with a vacancy and (b) a BN flake ($B_{12}N_{12}H_{12}$). B and N atoms correspond to the largest and medium-sized dots, respectively. All color scales for the diffraction patterns in the right panel are the same as in Fig. 2.

hexagonal flake, a diffraction pattern with the same symmetry features should be obtained via electron WP scattering. As a comparison, we also examine circumcoronene with a vacancy defect without hydrogen passivation near the center as observed in a previous experiment [42]. The diffraction pattern is shown on the right of Fig. 3(a). The regular LEED pattern observed in Fig. 2(c) is found to be heavily modified and the sixfold symmetry of either the inner or outer spots is lost.

Next, we present the simulated diffraction pattern of the H-terminated BN flake ($B_{12}N_{12}H_{12}$) in Fig. 3(b). The impact point of the WP is the center of the flake. The bright spots of the threefold symmetry in the pattern are formed by the electron WP scattered by the B and N atoms. Although the simplest single scattering theory of plane waves with the first Born approximation for the system leads to the diffraction pattern with sixfold symmetry, which is similar to Fig. 2, it is not the case for the WP scattering with B and N atoms with different atomic scattering factors and charges, as shown here. While the conventional LEED analysis that takes account of multiple scattering with a full potential calculation explains the atomic-species dependent LEED in the periodic structures, the present WP method simultaneously extracts the local atomic geometry and the atomic species near the impact point. From the center of the spots in the pattern and the Bragg diffraction condition, the B-N distance is calculated to be 1.45 Å, which agrees well with the practically used value of 1.43 Å. The origin of the difference between the two values was described above.

It is noted that in all the above calculations the impact point is the center of the flake. Here, we describe the WP impact-point dependence of the diffraction pattern, using circumcoronene as an example. Three impact points, labeled O, P, and Q, are given in Fig. 4(a). The simulated diffraction patterns for impact point P and Q are shown in Fig. 4(b) and 4(c) respectively. That for point O was shown in Fig. 2(c). In contrast to the sixfold symmetry in the pattern for impact point O, the patterns for P and Q only have threefold symmetry.
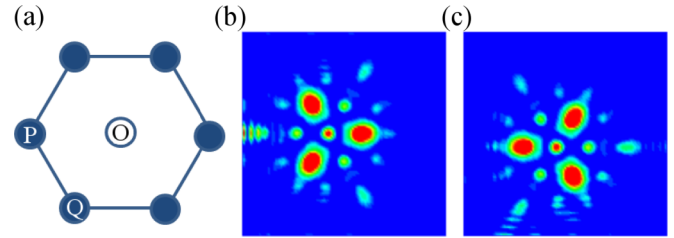
FIG. 4. (Color online) Impact-point dependent diffraction patterns. (a) A hexagon in the circumcoronene. The three impact points are indicated by O, P, and Q. The patterns for the impact points P and Q are given respectively in (b) and (c), while that for O is given in Fig. 2(c).

This is because the electron WP hitting the point O can see six nearest-neighbor C atoms, while the WPs hitting P and Q can only see three nearest-neighbor C atoms. Therefore, the diffraction pattern for O is similar to the regular LEED pattern of graphene generated by the scattering of plane-wave electrons, but this is not the case for the points P and Q. We expect that increasing the WP width will recover the sixfold symmetry in the diffraction pattern regardless of the impact point.

Lastly, we present the results of the electronic excitations in the target nanoflake upon impact of the electron WP, using Eqs. (6)–(9). We observe the electron density oscillations in the plane parallel to the flake when the WP hits the second C-C bond center from the edge of the flake in Fig. 2(c). The dipole excitation, $\sigma_x^d(\omega)$, due to the collision of a WP with a kinetic energy of 200 eV is given in Fig. 5(a). A few dip structures in the low-energy region with negative values of σ_x^d are caused by the transient behavior of the charge oscillation induced by the electron impact. Nevertheless, the peaks at around 2.5 and 5.2 eV are expected to have physical origins attributed to the electronic excitations discussed below.

To interpret the cause of the peaks, we calculated the optical absorption cross section of the circumcoronene by using an external optical field in the form of a δ function in the linear response regime [8]. The result is given in Fig. 5(b). Peaks at 2.3 and about 5.0 eV appeared in the low-energy region and
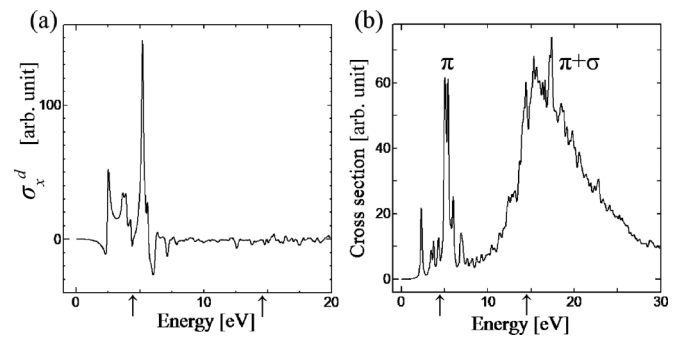
FIG. 5. (a) Dipole excitation in a circumcoronene caused by an electron WP with a kinetic energy of 200 eV and (b) optical absorption cross section in a circumcoronene caused by an external optical field in the form of a δ function in the linear response regime. The excitation energies of π and $\pi + \sigma$ plasmons observed in the EELS experiment [44] are indicated by arrows.

the highest peak in the high-energy region appeared at 17.4 eV. Similar spectra have been reported in a theoretical study [43]. We confirmed that the peak at about 5.0 eV in (b) can be attributed to a π plasmon, by observing the orbital character in the time evolution of the charge oscillation. The excitation at 17.4 eV in (b), which is not present in (a), is interpreted as a $\pi + \sigma$ plasmon excitation by a previous calculation [43]. Both peaks were observed in an experiment of the electron energy loss spectra (EELS) [44] and the peak positions are indicated by arrows in Fig. 5.

Apart from the broad peak that is missing in (a), a comparison of the spectra in Fig. 5 reveals that the spectra in the low-energy region of 5(a) originate from dipole excitations and the peak at 5.2 eV is a signature of a π plasmon excited by the WP impact. Since the present study is the first simulation of the dipole excitations by inelastic electron scattering with graphene nanoflakes, it is significant to verify that a graphene plasmon can be excited by an electron collision. Of course, further detailed analysis is required to confirm the one to one correspondence between the spectra of (a) and (b): First, we need longer simulation time to determine the mode frequency accurately; Second, it might be necessary to increase the incident energy or adjust the incident angle of the WP hitting on the target, so as to exert an electric field mimicking a δ-function form and satisfy the selection rules for the dipole excitations.

The above results show that TDDFT is promising for the simulation of electron scattering processes. Here, we note how our approach can be further improved in future work. One is on the exchange-correlation approximation. It is known that the contributions of the scattering phase-shift are not well captured by the ALDA [45]. Also, the electron scattering problem considered here is beyond the linear response; thus, the use of the ALDA becomes more challenging, although it is shown to be plausible for the present nanoflake systems. Owing to the remarkable efficiency of the ALDA, it is highly desirable to clarify its applicability to more extensive topics of

electron scattering problems, together with a comparison with other popular functionals, such as PBE [46], B3LYP [47], HSE [48] and long-range corrected (LC) [49] functionals, as well as "exact" ones like EXX [50]. The other improvement to our approach can be made through the use of the absorbing boundary condition (ABC). In the present study, the results were obtained without the use of ABC, but with a check on the sufficiency of the box size by analyzing the dispersion of the WP during the simulation of the LEED patterns. As the time-integration accuracy of TDDFT has been ensured in the present study, it is desirable to use the ABC in future work for long-time simulations with a box of a even smaller size.

In conclusion, the real-time and real-space TDDFT simulation of an electron WP scattered by a nanoflake has elucidated that the diffraction patterns obtained can reflect both the periodicity (long-range order) and the inhomogeneity (local atomic structure) of a target. This is important for the structural determination of nanosurfaces. The electronic excitations in the graphene nanoflake upon impact of the electron WP were also observed. Comparing the dipole response induced by electron scattering with the optical absorption spectra, the excitation in the low-energy region was found to correspond to π plasmons calculated by the TDDFT in the linear response framework. The present technique can be straightforwardly applied to the simulation of transmission electron microscopy for NBED using electron WPs with high kinetic energies. We have shown that the TDDFT simulation of electron scattering is a valuable tool for the analysis of atomic geometry and electronic excitations of nanosurfaces.

[1] E. Runge and E. K. U. Gross, Phys. Rev. Lett. **52**, 997 (1984).

[2] K. Burke, J. Werschnik, and E. K. U. Gross, J. Chem. Phys. **123**, 062206 (2005).

[3] M. Petersilka, U. J. Gossmann, and E. K. U. Gross, Phys. Rev. Lett. **76**, 1212 (1996).

[4] M. E. Casida, in *Recent Advances in Density Functional Methods*, *Part I*, edited by D. P. Chong (World Scientific, Singapore, 1995), p. 155.

[5] M. E. Casida, in *Recent Developments and Applications of Modern Density Functional Theory*, edited by J. M. Seminario (Elsevier, Amsterdam, 1996), p. 391.

[6] M. E. Casida, C. Jamorski, K. C. Casida, and D. R. Salahub, J. Chem. Phys. **108**, 4439 (1998).

[7] I. Vasiliev, S. Öğüt, and J. R. Chelikowsky, Phys. Rev. Lett. **82**, 1919 (1999).

[8] K. Yabana and G. F. Bertsch, Phys. Rev. B **54**, 4484 (1996).

[9] M. A. L. Marques, X. López, D. Varsano, A. Castro, and A. Rubio, Phys. Rev. Lett. **90**, 258101 (2003).

[10] C. Hu, H. Hirai, and O. Sugino, J. Chem. Phys. **127**, 064103 (2007).

[11] K. Tada and K. Watanabe, Phys. Rev. Lett. **88**, 127601 (2002).

[12] D. Utsugi, C. Hu, and K. Watanabe, Appl. Phys. Express **5**, 105101 (2012).

[13] M. van Faassen, A. Wasserman, E. Engel, F. Zhang, and K. Burke, Phys. Rev. Lett. **99**, 043005 (2007).

[14] A. Wasserman and K. Burke, in *Time-Dependent Density Functional Theory*, edited by M. A. L. Marques, C. A. Ullrich, F. Nogueira, A. Rubio, K. Burke, and E. K. U. Gross (Springer Berlin, 2006), p. 493.

[15] P. J. Rous, J. B. Pendry, D. K. Saldin, K. Heinz, K. Müller, and N. Bickel, Phys. Rev. Lett. **57**, 2951 (1986).

[16] E. A. Soares, C. M. de Castilho, and V. E. de Carvalho, J. Phys.: Condens. Matter **23**, 303001 (2011).

[17] H. Wu, J. Wang, R. So, and S. Y. Tong, J. Phys.: Condens. Matter **19**, 386203 (2007).

[18] G. M. Gavaza, Z. X. Yu, L. Tsang, C. H. Chan, S. Y. Tong, and M. A. Van Hove, Phys. Rev. Lett. **97**, 055505 (2006).

[19] G. M. Gavaza, Z. X. Yu, L. Tsang, C. H. Chan, S. Y. Tong, and M. A. Van Hove, Phys. Rev. B **75**, 235403 (2007).

[20] J. Onoda, T. Kanaoka, M. Kumon, and S. Mizuno, e-J. Surf. Sci. Nanotech. **10**, 292 (2012).

[21] A. Hirata, P. Guan, T. Fujita, Y. Hirotsu, A. Inoue, A. R. Yavari, T. Sakurai, and M. Chen, Nat. Mater. **10**, 28 (2011).

[22] P. Hohenberg and W. Kohn, Phys. Rev. **136**, B864 (1964).

[23] W. Kohn and L. J. Sham, Phys. Rev. **140**, A1133 (1965).

[24] N. Troullier and J. L. Martins, Phys. Rev. B **43**, 1993 (1991).

[25] K. Kobayashi, Comput. Mater. Sci. **14**, 72 (1999).

[26] J. P. Perdew and A. Zunger, Phys. Rev. B **23**, 5048 (1981).

[27] S. Kurth and G. Stefanucci, Phys. Rev. Lett. **111**, 030601 (2013).

[28] C. Toher, A. Filippetti, S. Sanvito, and K. Burke, Phys. Rev. Lett. **95**, 146402 (2005).

[29] H. Zhang, Y. Miyamoto, and A. Rubio, Phys. Rev. Lett. **109**, 265505 (2012).

[30] J.-A. Yan, J. A. Driscoll, B. K. Wyatt, K. Varga, and S. T. Pantelides, Phys. Rev. B **84**, 224117 (2011).

[31] Concerning the relevance of a WP scattered by a target to an electron beam in a LEED experiment, a train of WPs such as the stroboscopic WP scheme for steady current as recently proposed in Ref. [32] would be more realistic. To construct LEED patterns theoretically, however, the phase of the incident electron wave function has to be assigned, which is more essential for diffraction than for steady current. For this reason, a single WP in the present simulation can extract the essence of the Bragg diffraction condition upon electron scattering.

[32] P. Bokes, F. Corsetti, and R. W. Godby, Phys. Rev. Lett. **101**, 046402 (2008).

[33] The numerical accuracy of the fourth-order Taylor expansion approximation for the time evolution operator is given by the relative error in the electron number at the end of the simulation, which is 0.001% in the present study and does not influence the main results.

[34] The dipole excitation here is calculated from the imaginary part of the Fourier transform of the dipole moment, simply in analogy to the procedure of photoabsorption. In order to go beyond the linear regime, the more appropriate observable is the power spectrum, which is the absolute squared Fourier transform of the dipole moment. It is known that the spectral analysis in term of the power spectrum gives valuable insight when interpreted carefully [35–37].

[35] C. A. Ullrich, *Time-Dependent Density-Functional Theory: Concepts and Applications* (Oxford University Press, Oxford, 2011).

[36] F. Calvayrac, P. G. Reinhard, E. Suraud, and C. A. Ullrich, Phys. Rep. **337**, 493 (2000).

[37] F. Calvayrac, P. G. Reinhard, and E. Suraud, Ann. Phys. **255**, 125 (1997).

[38] H. Hayashi and Y. Udagawa, in *Charged Particle and Photon Interactions with Matter: Recent Advances, Applications, and Interfaces*, edited by Y. Hatano, Y. Katsumura, and A. Mozumder (CRC, Boca Raton, 2011), p. 88.

[39] S. M. Silverman, Phys. Rev. **111**, 1114 (1958).

[40] Y. Pan, H. Zhang, D. Shi, J. Sun, S. Du, F. Liu, and H.-J. Gao, Adv. Mater. **21**, 2777 (2009).

[41] K. Sugawara, K. Kanetani, T. Sato, and T. Takahashi, AIP Advances **1**, 022103 (2011).

[42] A. Hashimoto, K. Suenaga, A. Gloter, K. Urita, and S. Iijima, Nature (London) **430**, 870 (2004).

[43] H. Yin and H. Zhang, J. Appl. Phys. **111**, 103502 (2012).

[44] T. Eberlein, U. Bangert, R. R. Nair, R. Jones, M. Gass, A. L. Bleloch, K. S. Novoselov, A. Geim, and P. R. Briddon, Phys. Rev. B **77**, 233406 (2008).

[45] M. van Faassen and K. Burke, Phys. Chem. Chem. Phys. **11**, 4437 (2009).

[46] J. P. Perdew, K. Burke, and M. Ernzerhof, Phys. Rev. Lett. **77**, 3865 (1996).

[47] P. J. Stephens, F. J. Devlin, C. F. Chabalowski, and M. J. Frisch, J. Phys. Chem. **98**, 11623 (1994).

[48] J. Heyd, G. E. Scuseria, and M. Ernzerhof, J. Chem. Phys. **118**, 8207 (2003).

[49] Y. Tawada, T. Tsuneda, S. Yanagisawa, T. Yanai, and K. Hirao, J. Chem. Phys. **120**, 8425 (2004).

[50] T. Kotani, Phys. Rev. Lett. **74**, 2989 (1995).